

# Coherent Light Scattering from Semicontinuous Silver Nanoshells Near the Percolation Threshold

C. A. Rohde, K. Hasegawa, and M. Deutsch

Oregon Center for Optics and Department of Physics, University of Oregon, Eugene, OR 97403

(Dated: October 17, 2019)

We report on measurements of visible extinction spectra of semicontinuous silver nanoshells grown on colloidal silica spheres. We find that thin, fractal shells below the percolation threshold exhibit geometrically tunable plasmon resonances. A modified scaling theory approach is used to model the dielectric response of such shells, which is then utilized to obtain the extinction cross section in a retarded Mie scattering formalism. We show that such spherical resonators support unique plasmon dynamics: in the visible there is a new regime of coherently driven cluster-localized plasmons, while crossover to homogeneous response in the infrared predicts a delocalized shell plasmon.

Noble-metal nano-scale shells are comprised of thin gold or silver films surrounding sub-micron dielectric cores. In recent years nanometer-scale metal particles have been the focus of extensive studies, owing mainly to large enhancements of surface-induced electric fields at the plasma resonance of the nanoparticles [1]. This unique optical response is well exemplified in the nanoshells' extinction spectra, which are governed by a geometrically tunable plasmon resonance. When the core diameter is in the sub-micrometer range, the optical response of the composite particle is tunable over the entire visible and near infrared spectrum [2]. This constitutes a powerful tool for custom-designing Raman [3] and surface-plasmon-based ultra sensitive optical sensors [4].

The strong optical resonance observed in spherical nanoshells is attributed to a delocalized shell plasmon, typically well-modelled by classical linear response to electromagnetic plane-wave scattering [5]. This was formulated by Aden and Kerker (AK) [6] as an extension to classical Mie scattering theory [7]. More refined theories utilizing ab-initio quantum mechanical modelling of metallic nanoshells have also verified this approach [8].

The existence of the spherical-shell plasmon relies on highly symmetric and uniform shell morphology, and is typically observed in nanoshells which are smooth and continuous. It has been previously shown that the extinction spectra of incomplete or highly fragmented nanoshells do not exhibit unique geometrical resonances, but are dominated instead by absorption resonances of the metal clusters on the sphere surfaces [9, 10, 11, 12].

In this Letter we present light scattering experiments of silica spheres coated with discontinuous silver nanoshells. We distinguish two shell morphologies with differing optical signatures. For thin, two-dimensional (2D) fractal shells, we show that the optical response of the metal is best described within the framework of percolation theory. We find that while these shells support mainly localized plasmon modes and are electrically insulating, distinct geometrical resonances are clearly present, due to coherent optical driving of cluster-localized plasmons. For thick (3D), conducting and porous shells classical, Maxwell Garnett (MG) theory is used instead to obtain the effective dielectric response of the shell. We show that in both cases, although the shells are locally highly irregular, observed fine resonances are still well modelled by the AK solution to Maxwell's equations for uniform core/shell systems.

Colloidal silica spheres (0.3 - 1 $\mu$ m diameter, 1 - 3% polydisperse) were coated with nanocrystalline silver shells using a Tollen's reagent method to form metalodielectric core/shell particles. In this reaction aqueous ammoniacal silver nitrate is mixed with an aldehyde reducing agent, leading to rapid precipitation of silver atoms. When performed with a slow reducing agent (here glucose) at temperatures below 5°C the reaction kinetics are dramatically slowed, resulting in controlled deposition of nanocrystalline silver, only at the spheres' interfaces. Typical reactions last 20-30min. After termination of the reaction the spheres are washed by repeated centrifugation and sonication to eliminate residual silver nanocrystals in solution. Despite the lack of surface functionalization, the silver adheres strongly to the silica spheres and does not separate during this process.

Transmission electron micrographs (TEM) of more than 200 coated spheres per data set are used to determine average shell thickness and polydispersity. We find that for thin coatings ( $\sim$ 20 - 30nm) ensemble polydispersities can remain as low as 2%, indicating a highly uniform deposition process. High resolution TEM analyses of isolated metal clusters indicate that the latter consist of aggregated silver nanocrystals 5 - 10nm in size.

Further characterization of the shells' morphologies utilizes high-resolution scanning electron micrographs (SEM). These reveal the non-contiguous nature of the thin shells, which we characterize in terms of their metal filling fraction,  $p$ , and a fractal dimension,  $D_f$ . SEM images as in Fig. 1(a) are first processed with a high pass fast Fourier transform filter to eliminate nonuniform background intensity variations across the sphere surface. Sphere curvature and shadowing effects are minimized by utilizing only a small portion of the exposed surfaces close to nadir, shown enclosed in the box in Fig. 1(a). The size of this area must be small enough to minimize shadowing effects, while still sufficiently large to provide statistical integrity. With a resolution-limited pixel size of  $\simeq$  2nm, we find that for coated

spheres of radius  $R$  a box size of  $(R^2/4) \simeq 200^2$  pixels satisfies this condition. Linear contrast enhancement and thresholding of the cropped section provide the binary image in Fig. 1(b). Visual inspection of such images suggests a strong resemblance to percolating planar metal films deposited under ultra-high vacuum, where both linear and nonlinear optical characteristics have been previously addressed [13, 14].

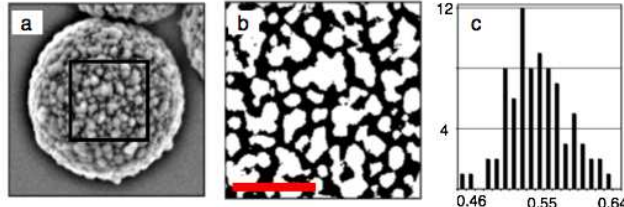


FIG. 1: (a) Scanning electron micrograph of  $1\mu\text{m}$  diameter silica sphere coated with a  $20\text{nm}$  silver quasi-shell. (b) Magnified view of the region inside the square in (a). Scale bar is  $200\text{nm}$ . (c) Histogram of  $p$ , generated from 80 images as (b).

Using a box-counting method [15] we find  $D_f = 1.72 \pm 0.06$ , indicating diffusion-limited aggregation in 2D [16]. Since this is below the fractal dimension of 2D percolating clusters,  $D_p = 1.89$  [17], we conclude that these shells lie slightly below the percolation threshold. We have verified this by measuring the average filling fraction  $\bar{p}$  of thin shells utilizing the processed SEM images. For an ensemble of  $\sim 100$  spheres we find  $\bar{p} = 0.55$ , shown in Fig. 1(c). Comparing to the experimental percolation threshold,  $p_c = 0.68$  [13], our thin shells have  $p \lesssim p_c$ .

This is supported by measurements of the bulk resistance of silver-coated spheres. A dense aggregate of spheres is formed by drying several concentrated drops of the sphere suspension between two gold electrodes separated by  $\sim 100\mu\text{m}$ . For shells  $20 - 40\text{nm}$  thick we measure a resistance  $R \sim 20\text{M}\Omega$ , while shells of thickness  $\geq 70\text{nm}$  exhibit a resistance of  $R \simeq 1\Omega$ . These are typical values, also obtained previously for the sheet resistance of planar thin metal films near the percolation threshold [13].

To optically characterize our core/shell composites we measured the extinction of freshly prepared, dilute aqueous suspensions using a UV/vis spectrometer. Spectra of sparsely coated spheres as in Fig. 2(a) exhibit a single peak centered near  $420\text{nm}$ . This is a signature of the excitation of the dipolar plasmon eigenmodes of individual, non-aggregated silver nanocrystals nucleated on the spheres [9, 11]. Due to the dilute metal surface-coverage, these modes do not couple to the weak Mie resonances of the dielectric spheres, and are therefore independent of sphere size. At the opposite extreme are densely coated spheres, shown in Fig. 2(b). In this limit the extinction is well-modelled by applying MG theory within the framework of Mie scattering, as discussed in a later section.

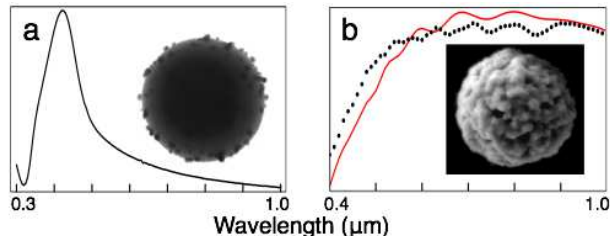


FIG. 2: (a) Extinction spectrum of sparsely coated  $1\mu\text{m}$  spheres (TEM inset) exhibiting a plasmon resonance at  $420\text{nm}$ . (b) Measured extinction (dots) and fitted AK model using MG theory (line) for a  $70\text{nm}$  thick shell (SEM inset).

Nucleation and aggregation of silver crystals onto the spheres result in an intermediate regime of discontinuous nanoshells of thickness  $20 - 30\text{nm}$ . Extinction spectra of spheres as in Fig. 1(a) reveal several distinct resonance peaks, all shifted from the single-particle plasmon resonance, as shown in Fig. 3(a). These are core/shell multipole modes, typically observed in high-contrast layered spherical particles. In addition, the inhomogeneously broadened enhanced red extinction tail present in fractal metal aggregates is strongly modulated here. These indicate that cluster-localized plasmon modes are interacting via cavity Mie resonances. Furthermore, varying the core size affects both peak number and positions, verifying the geometric nature of the resonances. In this new regime of coherently driven localized plasmons collective response of a strongly disordered shell is thus achieved.

A convenient method for modelling linear light scattering from core/shell particles employs AK-modified Mie formalism, which accounts for multiple scattering in layered concentric shells [6]. This method requires knowledge of the dielectric functions of core, shell and embedding medium materials. Using tabulated values for the dielectric

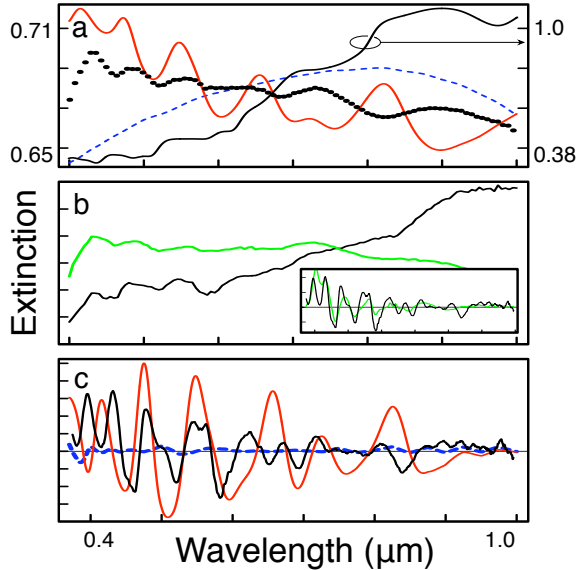


FIG. 3: (a) Comparison of normalized, averaged EMT (blue), and ST (red) extinction functions with measured spectra (dots). Also shown is the extinction obtained using the tabulated bulk silver dielectric function (black). (b) Normalized extinction spectra of two separate samples with same core/shell size parameters. Subtraction of computed background functions reveals universal spectral characteristics (Inset). (c) Comparison of background-subtracted, averaged extinction spectra for EMT (blue), ST (red) and measured data (black). All samples were 1 μm silica cores with 20 nm shells.

function of bulk silver to model the extinction coefficient exhibited serious discrepancies and failed to reproduce the experimental data, as seen in Fig. 3(a).

As previously indicated, our thin-shell samples are insulating, with shell filling fractions and morphology close to the percolation threshold. We therefore develop a method for modelling the optical response of such quasi-shells based on scaling theory (ST) for percolating planar metal films. The details of ST are described elsewhere [18], and only its germane points are summarized here. In this approach the scaling properties of a self-affine fractal network of conductors and insulators allow the definition of a scaling function [19]. A dielectric function  $\epsilon(\omega; L_\xi)$  is obtained in terms of this function and a characteristic length scale  $L_\xi$ , describing the largest length scale over which homogeneous averaging may occur.  $L_\xi$  is frequency-dependent, and is determined by the smallest of the relevant length scales: the percolation correlation length,  $\xi$ , or the optical coherence length  $L(\omega)$ , given respectively by

$$\xi \propto (|p - p_c|/p_c)^{-\nu} \quad (1a)$$

$$L(\omega) \propto \omega^{-1/(2+\theta)} \quad (1b)$$

For a 2D system near percolation the critical exponent is  $\nu = 4/3$ , and  $\theta = 0.79$ . Dielectric functions  $\epsilon_i$  and  $\epsilon_c$ , corresponding to insulating and conducting components of the metal film, respectively, are then calculated for each length scale  $L_\xi(\omega)$ .

The main difference between near-percolation planar films and our nanoshells stems from the closed shell geometry, which introduces correlations between film components that are otherwise uncorrelated in an open, planar configuration. This allows coherent driving of cluster-localized plasmon resonances through multipole electromagnetic cavity-modes, clearly resolved in the extinction spectra. We account for this cluster-coupling by defining the shell-averaged dielectric function

$$\epsilon_{\text{shell}}(\omega) = \langle \epsilon(\omega; L_\xi) \rangle = p\epsilon_c(\omega, L_\xi) + (1-p)\epsilon_i(\omega, L_\xi), \quad (2)$$

which is then utilized to calculate the extinction cross section in the AK formalism.

The resulting effective dielectric function exhibits characteristics that are strikingly different from those of both bulk and nanocrystalline silver. Most importantly, in the visible and near infrared (IR) spectral range Eq. (2) yields

positive values for  $\text{Re}[\epsilon_{\text{shell}}(\omega)]$  and relatively large values for  $\text{Im}[\epsilon_{\text{shell}}(\omega)]$ , implying a *lossy dielectric response*. This is typical of disordered metal films below the percolation threshold. This function is then seen to cross over to negative values in the IR. For common embedding dielectrics the crossover to metallic behavior occurs at  $\lambda \sim 1.5 - 2\mu\text{m}$ . This is related to a crossover from inhomogeneous to homogeneous optical response, which we calculate to occur near  $\lambda_{\xi} \sim 650\text{nm}$  in our samples [13]. At wavelengths much greater than  $\lambda_{\xi}$  the shell may be treated as optically homogeneous. The consequences of this are discussed in a later section.

The physical properties of composite materials are often treated using an effective-medium approach. This method asserts that when spatial inhomogeneities manifest on scales much smaller than the relevant length scale in the system, here the optical wavelength, average homogeneous treatment is justified. However, close enough to the percolation threshold this has been shown to break down [13, 20, 21]. We have also examined Bruggeman effective medium theory (EMT), which is best suited for systems near percolation [22, 23], as a plausible model for the shells' dielectric response. The effective dielectric function,  $\epsilon_{\text{eff}}$  is given by

$$p \frac{\epsilon_m - \epsilon_{\text{eff}}}{g\epsilon_m + (1-g)\epsilon_{\text{eff}}} + (1-p) \frac{\epsilon_d - \epsilon_{\text{eff}}}{g\epsilon_d + (1-g)\epsilon_{\text{eff}}} = 0 \quad (3)$$

where  $\epsilon_m$  and  $\epsilon_d$  are known dielectric functions of the interpenetrating metal and the dielectric, respectively, and  $g = 0.68$  is the depolarization factor. Using measured values of  $p$  we obtain an expression for  $\epsilon_{\text{eff}}$ , which is then utilized to calculate the extinction cross section as described above. For the relevant experimental parameters  $\epsilon_{\text{eff}}$  is a positive function over the entire EM spectral range, implying non-metallic response. As a final step for both ST and EMT approaches, the calculated extinction cross sections are averaged over the measured filling fraction  $p$  and sphere size distributions, and are plotted together for comparison in Fig. 3(a).

Close inspection of the two models reveals discrepancies in the general trend of the functions, with ST better following the data. Most importantly, the number of core/shell resonances, as well as their position and contrast, are not well-described by EMT. It is interesting to note that data taken from different samples may exhibit opposite background trends, as shown in Fig. 3(b). This is attributed mainly to various degrees of nanocrystal aggregation present in each batch, where increased aggregation results in a broad, enhanced red absorption tail. To properly account for this we therefore fit a background continuum function to each data set using boxcar averaging of the normalized extinction spectra. Subtraction of each continuum function from its respective spectrum reveals excellent agreement between the prominent spectral features, as shown in Fig. 3(b) (inset). In Fig. 3(c) we plot the normalized background-subtracted spectra, which may then be further analyzed using bandpass spectrophotometry. It is clearly seen that while ST properly reproduces the experimental results, EMT cannot account for the observed geometrical resonances.

As shell thickness increases through deposition of additional silver, we observe shifting of the core/shell resonances as shown in Fig. 2(b). High-resolution SEM micrographs indicate that the increase in shell thickness is accompanied by additional filling of interparticle voids, as well as further coarsening of the shells. Shells thicker than 50nm are therefore better treated as dense 3D aggregates of silver nanocrystals, with metal filling fractions estimated at  $0.8 \lesssim p \lesssim 0.9$ . Average measured polydispersities of such nanoshells may still be as low as 5%. Extinction spectra reveal characteristics closely similar to those of continuous solid silver nanoshells. It is therefore possible to describe the effective dielectric response of the porous shell using the classical Maxwell Garnett model. The dielectric function  $\epsilon_{\text{MG}}$  is given now by

$$\epsilon_{\text{MG}} = \epsilon_m \left[ 1 + \frac{3(1-p)(\epsilon_d - \epsilon_m)/(\epsilon_d + 2\epsilon_m)}{1 - (1-p)(\epsilon_d - \epsilon_m)/(\epsilon_d + 2\epsilon_m)} \right], \quad (4)$$

describing a solid silver shell with  $1 - p$  volume fraction of spherical dielectric inclusions. Following our procedure for calculating the size-averaged extinction cross section, we obtain the plot shown in Fig. 2(b). We find that this model reproduces well our experimental observations.

An interesting discrepancy between ST and EMT emerges when the extinction calculations are extended into the IR range, as shown in Fig. 4. We find that ST predicts a broad IR absorption, while EMT exhibits a decaying Rayleigh extinction tail. The broad peak centered near  $3.2\mu\text{m}$  is due to a mostly dipolar shell plasmon resonance, as verified by numerical mode-decomposition of both absorption and scattering cross-sections. This is a consequence of the above mentioned crossover to metallic behavior in ST, which enables the excitation of a *delocalized* shell plasmon. We note that this IR resonance should be distinguished from anomalous IR absorption observed previously in metal-dielectric composites [24]. The latter originates from enhanced absorption in the embedding dielectric, due to intense local electric fields [25]. Here we assume both silica core and dielectric inclusions in the shell are lossless, therefore all absorption in this model is due to intrinsic losses in the metal shell.

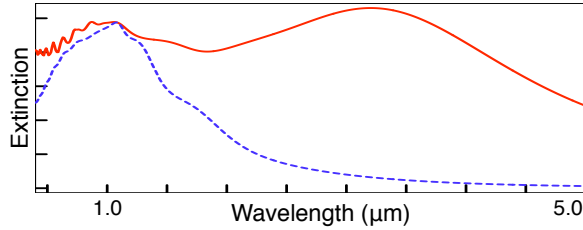


FIG. 4: Calculated extinction for ST (line) and EMT (dashed) for  $p = 0.55$ , 20nm silver shells on  $1\mu\text{m}$  diameter silica cores.

In summary, we have shown that extinction properties of semicontinuous silver nanoshells grown on dielectric cores unambiguously differ from previously reported smooth core/shell systems. We have demonstrated tuning of the plasmon resonance with shell growth - from a single dipolar mode in sparse coatings to multiple high order shell excitations in densely aggregated thick shells. We have identified an intermediate regime of thin fractal shells near the percolation threshold, where geometrically tunable plasmon resonances persist despite disorder and the shells' discontiguous character. A modified approach for modelling the dielectric response of fractal shells, based on scaling theory is consistent with experimental observations. We attribute this new resonant regime to cluster-localized plasmons, coherently driven by micro-resonator modes. Future work will address the predicted delocalized plasmon resonance, resulting from a crossover to homogeneous metallic response in the IR .

The authors thank J. Bouwman and S. Emmons for assistance with chemical syntheses. We also acknowledge helpful discussions with R. Haydock and G. Bothun. This work was supported by NSF Grant No. DMR-02-39273 and ARO Grant No. DAAD19-02-1-0286.

---

[1] M. Moskovits, Rev. Mod. Phys. **57**, 783 (1985).  
[2] S. J. Oldenburg et al., Chem. Phys. Lett. **288**, 243 (1998).  
[3] J. B. Jackson et al., Appl. Phys. Lett. **82**, 257 (2003).  
[4] S. Schultz et al., Proc. Nat. Acad. Sci. **97**, 996 (2000).  
[5] R. D. Averitt, D. Sarkar, and N. J. Halas, Phys. Rev. Lett. **78**, 4217 (1997).  
[6] A. L. Aden and M. Kerker, J. Appl. Phys. **22**, 1242 (1951).  
[7] G. Mie, Ann. Phys. **24**, 377 (1908).  
[8] E. Prodan and P. Nordlander, Nano Lett. **3**, 543 (2003).  
[9] T. Ji et al., Adv. Mater. **13**, 1253 (2001).  
[10] C. Graf and A. van Blaaderen, Langmuir **18**, 524 (2002).  
[11] D. I. Gittins et al., Adv. Mater. **14**, 508 (2002).  
[12] C. M. Aguirre et al., J. Phys. Chem. B **108**, 7040 (2004).  
[13] Y. Yagil et al., Phys. Rev. B **46**, 2503 (1992).  
[14] V. M. Shalaev and A. K. Sarychev, Phys. Rev. B **57**, 13265 (1998).  
[15] C. Douketis et al., Phys. Rev. B **51**, 11022 (1995).  
[16] P. Jensen et al., Phys. Rev. B **50**, 15316 (1994).  
[17] M. B. Isichenko, Rev. Mod. Phys. **64**, 961 (1992).  
[18] Y. Yagil et al., Phys. Rev. B **43**, 11342 (1991).  
[19] J. P. Straley, J. Phys. C **9**, 783 (1976).  
[20] D. Stroud, Phys. Rev. B **19**, 1783 (1979).  
[21] V. A. Shubin et al., Phys. Rev. B **62**, 11230 (2000).  
[22] D. Bruggeman, Ann. Phys. (Leipzig) **24**, 6736 (1935).  
[23] R. W. Cohen et al., Phys. Rev. B **8**, 3689 (1973).  
[24] R. P. Devaty, Phys. Rev. B **44**, 593 (1991).  
[25] M. Gadenne et al., Europhys. Lett. **53**, 364 (2001).